GALE: An Enhanced Geometry-Assisted Location Estimation Algorithm for NLOS Environments

Kai-Ten Feng, *Member*, *IEEE*, Chao-Lin Chen, and Chien-Hua Chen, *Student Member*, *IEEE*

Abstract—Mobile location estimation has attracted a significant amount of attention in recent years. The network-based location estimation schemes have been widely adopted based on the radio signals between the mobile device and the base stations. The two-step Least-Squares (LS) method has been studied in related research to provide efficient location estimation of the mobile devices. However, the algorithm results in insufficient accuracy for location estimation with the existence of Non-Line-Of-Sight (NLOS) errors. A Geometry-Assisted Location Estimation (GALE) algorithm is proposed in this paper with the consideration of different geometric layouts between the mobile device and its associated base stations. In order to enhance the precision of the location estimate, the GALE scheme is designed to incorporate the geometric constraints within the formulation of the two-step LS method. The algorithm can be utilized to estimate both the two-dimensional and the three-dimensional positions of a mobile device. The proposed GALE scheme can both preserve the computational efficiency from the two-step LS algorithm and obtain a precise location estimation under NLOS environments. Moreover, the Cramér-Rao Lower Bound (CRLB) for various types of measurement signals is derived to facilitate the performance comparison between different location estimation schemes. Numerical results illustrate that the proposed GALE algorithm can achieve better accuracy compared with other existing network-based location estimation schemes.

Index Terms—Wireless location estimation, two-step Least-Squares method, Non-Line-Of-Sight (NLOS) errors, Time-Of-Arrival (TOA), Angle-Of-Arrival (AOA).

1 Introduction

Wireless location technologies, which are designated to estimate the position of a Mobile Station (MS), have drawn a lot of attention over the past few decades. Different types of Location-Based Services (LBSs) have been proposed and studied, including the emergency 911 (E-911) subscriber safety services [1], location-based billing, the navigation system, and applications for the Intelligent Transportation System (ITS) [2]. Due to the emergent interests in the LBSs, it is required to provide enhanced precision in the location estimation of an MS under different environments.

A variety of wireless location techniques have been studied and investigated [3], [4], [5]. Network-based location estimation schemes have been widely proposed and employed in wireless communication systems. These schemes locate the position of the MS based on the measured radio signals from its neighborhood Base Stations (BSs). The representative algorithms for the network-based location estimation techniques are the Time-Of-Arrival (TOA), the Time Difference-Of-Arrival (TDOA), and the Angle-Of-Arrival (AOA). The TOA scheme estimates the MS's location by measuring the arrival time of the radio signals coming from different wireless BSs, whereas the TDOA method measures the time difference between the arriving radio signals. The AOA technique is conducted within the BS by observing the arriving angles of the signals coming from the MS. The equations associated with the network-based location estimation schemes are inherently nonlinear. The uncertainties induced by the measurement noises make it more difficult to acquire the estimated MS position with tolerable precision. The two-step Least-Squares (LS) scheme [6] has been studied to provide reasonable accuracy for location estimation with its efficient two-step calculation. However, the algorithms based on the two-step LS method are primarily feasible for location estimation under Line-Of-Sight (LOS) environments. Non-Line-Of-Sight (NLOS) situations, which occur mostly under urban or suburban areas, greatly affect the precision in most location estimation schemes.

In this paper, an efficient Geometry-Assisted Location Estimation (GALE) algorithm is proposed to obtain the location estimation of the MS, especially under NLOS environments. The proposed GALE scheme integrates the geometric information from the cell layout into the conventional two-step LS algorithm. The MS's position is obtained by confining the estimation based on the signal variations and the geometric layout between the MS and the BSs. Both the 2D and 3D locations of the MS can be estimated using the proposed GALE scheme. A reasonable location estimation can be acquired within two computing iterations even with the existence of NLOS errors. Furthermore, the Cramér-Rao Lower Bound (CRLB) associated with different distributions of measurement inputs is also

• *The authors are with the Department of Communication Engineering, National Chiao Tung University, 1001 Ta Hsueh Road, Hsinchu, Taiwan 300, ROC. E-mail: ktfeng@mail.nctu.edu.tw, {sart.cm92g, chchen.cm93g}@nctu.edu.tw.*

Manuscript received 21 Sept. 2006; revised 13 Mar. 2007; accepted 30 May 2007; published online 19 June 2007.
For information on obtaining reprints of this article, please send e-mail to: tmc@computer.org, and reference IEEECS Log Number TMC-0241-0906.
Digital Object Identifier no. 10.1109/TMC.2007.70721.

derived. The CRLB will be utilized as a lower bound to compare the performance of the location estimation algorithms. Different cases are illustrated in simulations in order to demonstrate the effectiveness of the GALE algorithm. Compared with other existing schemes, the numerical results show that the GALE approach can acquire higher accuracy for the location estimation of the MS.

The remainder of this paper is organized as follows: Section 2 describes related work for wireless location estimation. The proposed GALE algorithm is explained in Section 3 for both the 2D and the 3D location estimation. The performance evaluation of the proposed scheme is conducted in Section 4 via simulations. Section 5 draws the conclusions.

2 Related Work

Different location estimation schemes have been proposed to acquire the MS's position. Various types of information (for example, the signal traveling distance, the received angle of the signal, and the Receiving Signal Strength (RSS)) are involved to facilitate the algorithm design for location estimation. The primary objective in most location estimation algorithms is to obtain higher estimation accuracy with promoted computational efficiency. Superresolution (or high-resolution) schemes are proposed in [7], [8], [9], and [10]. The scheme studied in [7] considers arbitrarily located antennas and a particular covariance matrix within a noisy environment. The covariance matrix is composed of various types of properties, including gain, phase, frequency, polarization, and AOA information. The subspace method utilized in the superresolution schemes estimates the components of the covariance matrix based on an eigenanalysis. A well-known superresolution algorithm is the MUltiple SIgnal Classification (MUSIC) [8]. It is experimentally illustrated to be a robust solution for location estimation, especially for a near-far environment. However, it has also been shown in [9] and [10] that the drawbacks of the MUSIC approach include 1) its comparably high sensitivity to large noise and 2) its complexity in computation.

The beamforming system is a space-time processor that operates on the output of a sensor array. It provides a spatial filtering capability that enhances the amplitude of a coherent signal associated with the surrounding noises. Since the conventional beamforming technique is sensitive to the estimation error for the MS's position, a combination of localization and beamforming is proposed as in [11]. It increases the robustness to location errors without sacrificing the computation efficiency. An enhanced algorithm for simultaneous multisource beamforming and adaptive multitarget tracking is studied in [12]. The correlation between the adaptive minimum variance beamforming and the optimal MS localization is investigated in [13]. However, the complication of the beamforming system makes the associated location estimation techniques difficult to be practically realized.

Instead of exploiting the spatial and temporal information of the signal, the RSS measurements can be utilized for the estimation of the MS's position [14], [15], [16], [17], [18]. The location fingerprinting technique [14], [15] involves both the offline and online phases. A location grid that is related to a signal signature database for a specific service area is developed in the offline phase, whereas a measured RSS vector at the MS is delivered to the central server to compare with the location grid in the online phase. Moreover, a hybrid algorithm that combines the radio frequency (RF) propagation loss model is proposed both to mitigate the requirement of the training data and to adjust the configuration changes [16]. The scheme proposed in [17] considers one-to-one mapping between the RSS measurement and the MS's location. The location of the MS can be estimated by adopting the LS method with the minimization of a predefined cost function. The hybrid RSS method [18] identifies the location of the indoor users by exploiting the distribution of the RSS Aggregate (RSSA) measured from both the indoor and the outdoor handsets. The location information can therefore be recorded into a database with different signal levels. However, it is obvious to recognize that a considerable size of the database is, in general, required for the location techniques based on the RSS signals.

On the other hand, the ray-tracing and ray-launching techniques are the two ray optical approaches for location estimation. The radio signals that are launched from a transmitter and reflected or diffracted by various objects are aggregated in a receiver. The field strength and the signal propagation can therefore be predicted [19], and Chang and Kim [20] further proposed an efficient algorithm for prediction. Three-dimensional indoor radio propagation models are developed in [21] and [22]. Experimental formulas from extensive measurements of both urban and suburban propagation losses are studied in [23] and [24]. However, tremendous computation of the field strength is involved at the receiver as the numbers of the reflective and the diffractive signals are increased. Moreover, the well-adopted discrete launching angle may result in unattainable radio signals to the receiver.

There are also different approaches exploiting linearized methods to achieve computing efficiency while obtaining an approximate estimation of the MS's position. The Taylor Series Expansion (TSE) method was utilized in [25] to acquire the location estimation from the TDOA measurements. Moreover, an enhanced TSE technique [26] has been proposed to explicitly consider the NLOS errors within its formulation. This approach estimates the MS's position by minimizing a cost function constructed by the intersecting points based on the cell layout. Both of these methods require iterative processes to obtain the location estimate from a linearized system. The major drawback of TSE-based schemes is that they may suffer from the convergence problem due to an incorrect initial guess of the MS's position. The two-step LS method was adopted to solve the location estimation problem from the TOA [6], the TDOA [27], and the TDOA/AOA measurements [28]. It is an approximate realization of the Maximum Likelihood (ML) estimator and does not require iterative processes. The two-step LS scheme is advantageous in its computational efficiency with adequate accuracy for location estimation.

However, the scheme is demonstrated to be feasible only for acquiring the position of the MS under LOS circumstances.

Instead of utilizing Circular-Line-Of-Position (CLOP) methods (for example, the TSE and the two-step LS schemes), the Linear-Line-Of-Position (LLOP) approach is presented as a different interpretation for the cell geometry from the TOA measurements. Since two TOA measurements that intersect at two points will generate a connecting line, two independent lines will be created by using three BSs in the scenario of 2D location estimation. Therefore, the LS method can be adopted to estimate the location of the MS. The detailed algorithm of the LLOP approach can be obtained by using the TOA measurements in [29] and the hybrid TOA/AOA measurements in [30]. On the other hand, the Kalman-based Interacting Multiple Model (IMM) smoother [31] is proposed for the location estimation based on the TOA measurements. The technique employed the three-stage Kalman filters, which can discriminate the NLOS error from its LOS signal. However, an appropriate selection of the parameters within the Kalman models is required to preserve the precision for location estimation. The Range Scaling Algorithm (RSA) proposed in [32] alleviates the NLOS errors by considering the cell layout between the MS and its associated BSs. A constrained nonlinear optimization approach is adopted to obtain an improved location estimate for the MS. However, the RSA approach involves the requirement of solving an optimization problem based on a nonlinear objective function. The inefficiency incurred by the algorithm may not be feasible to be applied in practical systems.

It can be found from previous work that some location estimation algorithms involve complicated computation or additional database and infrastructures, whereas others are only suitable for specific situations (for example, LOS environments or special areas). Not much effort has been dedicated in the estimation of a 3D MS's position, which can be essential for scenarios within a metropolitan valley or inside a building. The GALE algorithm proposed in this paper preserves the computational efficiency from the two-step LS method, whereas the integrated information from the cell geometry extends the estimation capability under NLOS environments. In addition to the 2D setting of the GALE scheme, the extended 3D GALE algorithm will also be validated in this paper to provide sufficient precision for location estimation.

3 The Proposed GALE Algorithm

In this section, the proposed GALE scheme is described in detail. The mathematical modeling of the signal measurements are formulated in Section 3.1. Section 3.2 briefly summarizes the concept of the conventional two-step LS method. The proposed GALE algorithm in the form of 2D and 3D formulations is presented in Sections 3.3 and 3.4 with two different cases, that is, the TOA and the hybrid TOA/AOA measurements.

3.1 Modeling of Signal Measurements

In order to facilitate the design of the proposed GALE algorithm, the signal models for the TOA and the AOA measurements are presented in this section. The TOA measurement t_ℓ from the ℓth BS is obtained by

$$t_\ell = \frac{r_\ell}{c} = \frac{1}{c}(\zeta_\ell + n_\ell) = \frac{1}{c}(\zeta_\ell + n_{\ell,m} + n_{\ell,nl}), \tag{1}$$

where $\ell = 1, 2, \ldots, N$. Parameter c is the speed of light, and r_ℓ represents the measured relative distance between the MS and the ℓth BS. r_ℓ is contaminated with noises n_ℓ from the TOA measurement, which includes the measurement noise $n_{\ell,m}$ and the NLOS error $n_{\ell,nl}$. It is noted that the NLOS error $n_{\ell,nl}$ is a positive value due to the larger distance traversed by the NLOS effect. The noiseless relative distance ζ_ℓ between the MS and the ℓth BS is denoted as

$$\zeta_\ell = \|\boldsymbol{x} - \boldsymbol{x}_\ell\|, \tag{2}$$

where $\boldsymbol{x} = (x, y)$ represents the MS's position, and $\boldsymbol{x}_\ell = (x_\ell, y_\ell)$ is the location of the ℓth BS in the 2D setting, whereas $\boldsymbol{x} = (x, y, z)$ and $\boldsymbol{x}_\ell = (x_\ell, y_\ell, z_\ell)$ within the 3D formulation. On the other hand, the horizontal AOA measurement θ and the vertical AOA measurement ϕ can be obtained by

$$\theta = \theta_t + n_\theta = \tan^{-1}\left[\frac{y - y_1}{x - x_1}\right] + n_\theta, \tag{3}$$

$$\begin{aligned}\phi &= \phi_t + n_\phi \\ &= \tan^{-1}\left[\frac{z - z_1}{\sqrt{(x - x_1)^2 + (y - y_1)^2}}\right] + n_\phi,\end{aligned} \tag{4}$$

where θ and ϕ represent the measured horizontal and vertical angles between the MS and its home BS, that is, BS_1. It is noted that (x_1, y_1, z_1) corresponds to the coordinate of BS_1. θ_t and ϕ_t are the corresponding noiseless angles, whereas n_θ and n_ϕ are the measurement noises associated with θ and ϕ. It is suggested [28] that the AOA measurement should only be adopted with respect to the home BS due to the unreliable angle measurements with respect to the other BSs (that is, the signal degradation due to the near-far effect). Both the TOA and the AOA measurement models will be applied in the design of the proposed GALE algorithm under different scenarios.

3.2 The Two-Step Least Square (LS) Method

The two-step LS scheme is utilized as the baseline formulation for the proposed GALE algorithm. In this paper, the two-step LS method is extended from its original 2D setting [6], [27], [28] to the 3D formulation to facilitate the design of the proposed algorithm. The concept of the two-step LS method is to acquire an intermediate location estimate in the first step with the definition of a new variable β, which is mathematically related to the MS's position (that is, $\beta = x^2 + y^2$ in the 2D case and $\beta = x^2 + y^2 + z^2$ in the 3D case). At this stage, the variable β is assumed to be uncorrelated to the MS's position. This assumption effectively transforms the nonlinear equations for location estimation into a set of linear equations which can be directly solved by the LS method. Moreover, the elements within the associated covariance matrix are selected based on the standard deviation from the measurements. The

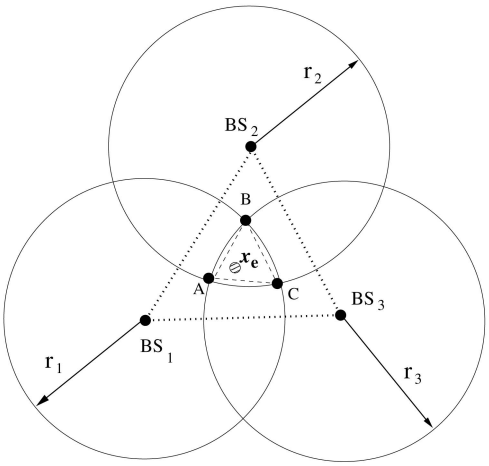

Fig. 1. The schematic diagram of the 2D TOA-based location estimation for NLOS environments.

variations within the corresponding signal paths are therefore considered to be within the problem formulation.

The second step of the method primarily considers the relationship that the variable β is equal to $x^2 + y^2$ (in the 2D case) or $x^2 + y^2 + z^2$ (in the 3D case), which was originally assumed to be uncorrelated in the first step. An improved location estimation can be obtained after the adjustment from the second step. The detail algorithm of the two-step LS method for location estimation can be found by using the TOA measurements [6], the TDOA measurements [27], and the hybrid TDOA/AOA measurements [28].

3.3 The Proposed 2D GALE Algorithm

The proposed 2D GALE algorithm associated with the applications within two different scenarios are described in this section. The concept of the GALE algorithm is to consider the geometric constraints between the MS and the BSs within the formulation of the two-step LS method. It is recognized that the range measurements are in general corrupted by both the measurement noises and the NLOS errors. The conventional two-step LS algorithm obtains a location estimate primarily by considering the measurement noises with gentle NLOS errors. The proposed GALE scheme, on the other hand, can manage the cases with the existence of considerable NLOS errors. The following two different cases (that is, the three-TOA measurements and the two TOA and one AOA measurements) are considered.

3.3.1 Three TOA Measurements

The TOA-based location estimation in the 2D setting is illustrated in Fig. 1. The measured distances between the BSs and the MS are denoted as r_ℓ for $\ell = 1$, 2, and 3. It is noted that the three circles that define the TOA measurements will intersect to a single point (that is, the MS's position) if the measurements are LOS and are free of the measurement noises. The overlap region confined within points A, B, and C (as shown in Fig. 1) is primarily incurred by the NLOS errors. It was observed that the location estimation by using the conventional two-step LS method may fall around the boundaries of the three arcs, AB, BC, and CA, that is, either inside or outside of these arcs. Since the overlap region (that is, constrained by points A, B, and C) grows as the NLOS errors are increased, the location estimation of the MS acquired by the two-step LS method will result in deficient accuracy (that is, the location estimate will fall around the boundaries of the enlarged arcs AB, BC, and CA).

Based on extensive field experiments [33], [34], it has been acquired that the mean and the standard deviation of the NLOS range error are in the order of 513 m and 436 m, respectively. Meanwhile, depending on the precision of the measuring facilities from both the BS and the MS sides, the measurement noise is considered at least one order less than that from the NLOS error. Therefore, it is generally assumed that the NLOS error is larger than the measurement noise in mobile location estimation [31]. The following proposition proves that the location of the MS should always fall inside the overlap region under an environment with large NLOS errors, that is, while the NLOS error is comparably larger than the absolute value of the measurement noise.

Proposition 1. *$\zeta_\ell \in \Re^+ \cup \{0\}$ is denoted as the noiseless relative distance between the MS and the ℓth BS for $\ell = 1, 2, \ldots, N$. $n_{\ell,m} \in \Re$ represents the measurement noise, and $n_{\ell,nl} \in \Re^+ \cup \{0\}$ is denoted as the NLOS error with respect to the ℓth BS. The measured relative distance between the MS and the ℓth BS is $r_\ell = \zeta_\ell + n_{\ell,m} + n_{\ell,nl}$. $\mathcal{C}_\ell = \{\boldsymbol{p} \in \Re | \, \|\boldsymbol{p} - \boldsymbol{x}_\ell\| < r_\ell\}$ denotes the set of points within the circular region centered at the location of the* BS_ℓ *with radius r_ℓ. If $n_{\ell,nl} > |n_{\ell,m}|$, the MS's position $\boldsymbol{x}$ will fall within the set $\mathcal{I} = \mathcal{C}_1 \cap \mathcal{C}_2 \cap \ldots \cap \mathcal{C}_N$ using N's TOA measurements.*

Proof. Since $n_{\ell,nl} > |n_{\ell,m}|$, it can be obtained that $n_{\ell,nl} - |n_{\ell,m}| > 0$. With the substitution of the inequality, the measured relative distance becomes $r_\ell = \zeta_\ell + n_{\ell,nl} + n_{\ell,m} \geq \zeta_\ell + n_{\ell,nl} - |n_{\ell,m}| = \zeta_\ell + (n_{\ell,nl} - |n_{\ell,m}|) > \zeta_\ell$. This inequality (that is, $\zeta_\ell < r_\ell$) indicates that the noiseless distance from the MS's position $\boldsymbol{x}$ to the location of BS_ℓ is less than the measured relative distance r_ℓ. It corresponds to the case that $\boldsymbol{x}$ should lie within the set $\mathcal{C}_\ell$, that is, $\boldsymbol{x} \in \mathcal{C}_\ell$. By using N's TOA measurements for the location estimation of the MS, $\boldsymbol{x}$ will be located within the intersecting set $\mathcal{I}$, that is, $\boldsymbol{x} \in \mathcal{I} = \mathcal{C}_1 \cap \mathcal{C}_2 \cap \ldots \cap \mathcal{C}_N$.□

Based on the proposition above, the primary objective of the proposed 2D GALE algorithm is to confine the location estimate within the overlap region by including the geometric constraints into the two-step LS method. As illustrated in Fig. 1, three BSs associated with the three TOA measurements are required for the location estimation of the MS. Since the objective of the proposed 2D GALE scheme is to confine the estimated MS's position within the region of ABC, the following constraint is defined:

Definition 1 (Virtual Distance). *The parameter γ is defined as a* virtual distance *between the MS's position and the three intersecting points A, B, and C:*

$$\gamma = \left[\sum_{\mu} \frac{1}{m} \|\boldsymbol{x} - \boldsymbol{x}_\mu\|^2 \right]^{1/2}, \tag{5}$$

where $\boldsymbol{x}$ is the MS's location, $\boldsymbol{x}_\mu$ represents the intersecting points around the overlap region, that is, $\boldsymbol{x}_\mu = \boldsymbol{x}_a$, $\boldsymbol{x}_b$, and $\boldsymbol{x}_c$

in this case, where $\boldsymbol{x}_a = (x_a, y_a)$, $\boldsymbol{x}_b = (x_b, y_b)$, *and* $\boldsymbol{x}_c = (x_c, y_c)$ *are the corresponding coordinates of points* A, B, *and* C. m *denotes the number of the intersecting points around the overlap region, that is,* $m = 3$ *in this case.*

It is noted that the value of γ varies as the three coordinates $\boldsymbol{x}_a$, $\boldsymbol{x}_b$, and $\boldsymbol{x}_c$ are changed. On the other hand, an expected MS's position $\boldsymbol{x}_e$ is chosen to be located within the triangular area ABC in order to fulfill the constraints from the geometric layout. The corresponding *expected virtual distance* γ_e can be defined as follows:

Definition 2 (Expected Virtual Distance). *The parameter* γ_e *is defined as the* expected virtual distance, *which is represented as*

$$\gamma_e = \left[\sum_{\mu} \frac{1}{m} \|\boldsymbol{x}_e - \boldsymbol{x}_\mu\|^2\right]^{1/2} = \gamma + n_\gamma, \tag{6}$$

where $\boldsymbol{x}_e$ *is the expected position of the MS and* n_γ *denotes the error induced by the computed deviation between* γ_e *and* γ.

The major objective of adapting the geometric constraint in the GALE algorithm is to minimize the cost function $f = \|\gamma - \gamma_e\|$ with constraints as in (6), that is, to minimize the deviation between the *virtual distance* γ and the *expected virtual distance* γ_e. The selection of the expected MS's position $\boldsymbol{x}_e$ is obtained by considering the signal variations from the three TOA measurements. The coordinates of $\boldsymbol{x}_e = (x_e, y_e)$ are chosen with different weights (w_1, w_2, w_3) with respect to the A, B, and C points of the triangle as follows:

$$\boldsymbol{x}_e = \sum_{k=1}^{m} w_k I_k, \tag{7}$$

where I_k denotes the intersecting points from the TOA measurements, that is, $I_1 = \boldsymbol{x}_a$, $I_2 = \boldsymbol{x}_b$, and $I_3 = \boldsymbol{x}_c$. The weighting coefficients w_k are defined as

$$w_k = \frac{\sigma_k^2/d_k}{\sum_{i=1}^{m}(\sigma_i^2/d_i)} \tag{8}$$

for $k = 1$, 2, and 3. The selection criterion for the weight w_k in (8) relies on the effects from both the standard deviations σ_k and the relative distance d_k, which are explained as follows:

1. σ_1, σ_2, and σ_3 are denoted as the corresponding standard deviations obtained from the three TOA measurements, that is, $\sigma_1 = \sigma_{r_1}$, $\sigma_2 = \sigma_{r_2}$, and $\sigma_3 = \sigma_{r_3}$. For the measurement r_1 (as shown in Fig. 1), the MS's position should be located around the boundary of the circle with the radius r_1 without the existence of the NLOS errors. If the standard deviation σ_{r_1} of the measurement r_1 is comparably large, it indicates that the true position of the MS should move toward the inside of the circle boundary of the radius r_1 due to the NLOS errors. Consequently, the weight w_1 is assigned with a larger value, which specifies that the position of the MS should move toward the endpoint A of the triangle. The design concept can be applied to the selection of the other two weights, w_2 and w_3, in the same manner.
2. d_k is utilized to denote the summed relative distances, that is,

$$d_k = \sum_{j=1, j\neq k}^{m} \|I_k - I_j\| \tag{9}$$

represents the summation of the relative distances from the kth intersecting point to the other points (for example, d_1 corresponds to the relative distances from point A to points B and C). The weight d_k is utilized to consider the influence from the geometrical shape of the triangular area ABC. For example, point A is located at a longer distance away from points B and C as the value of d_1 is comparably larger; it will be difficult for the expected MS's position $\boldsymbol{x}_e$ to move from the circular boundary of the radius r_1 toward endpoint A. As a result, the weighting coefficient w_1 in (8) will be assigned with a smaller value since it is inversely proportional to d_1. On the other hand, if the relative distance between points A, B, and C are comparably similar, distances d_1, d_2, and d_3 will result in similar values. The distance effect on the weights w_k is considered neglected.

Based on the appropriate selection of the weighting coefficients, the expected MS's position $\boldsymbol{x}_e$ is obtained. The *expected virtual distance* γ_e can therefore be computed from (6). The proposed 2D GALE algorithm is formulated by solving the two-step LS problem with the additional geometric constraint. The solution is obtained by minimizing both 1) the errors coming from the three TOA measurements (as in (1)) and 2) the deviation between the *expected virtual distance* and the *virtual distance* (as in (6)). By rearranging and combining (1) and (6) in a matrix format, the following equation can be obtained:

$$\mathbf{H}\boldsymbol{z} = \mathbf{J} + \psi, \tag{10}$$

where

$$\boldsymbol{z} = [x \quad y \quad \beta]^T, \tag{11}$$

$$\mathbf{H} = \begin{bmatrix} \mathbf{H}_{TOA}^{3\times 3} \\ \mathbf{H}_{\gamma}^{1\times 3} \end{bmatrix} = \begin{bmatrix} -2x_1 & -2y_1 & 1 \\ -2x_2 & -2y_2 & 1 \\ -2x_3 & -2y_3 & 1 \\ -2x_\gamma & -2y_\gamma & 1 \end{bmatrix}, \tag{12}$$

$$\mathbf{J} = \begin{bmatrix} \mathbf{J}_{TOA}^{3\times 1} \\ \mathbf{J}_{\gamma}^{1\times 1} \end{bmatrix} = \begin{bmatrix} r_1^2 - \kappa_1 \\ r_2^2 - \kappa_2 \\ r_3^2 - \kappa_3 \\ \gamma_e^2 - \kappa_\gamma \end{bmatrix}. \tag{13}$$

The corresponding coefficients are given by

$$\begin{aligned} \beta &= x^2 + y^2, \\ \kappa_\ell &= x_\ell^2 + y_\ell^2 \qquad \text{for } \ell = 1, 2, 3, \\ x_\gamma &= \frac{1}{3}(x_a + x_b + x_c), \\ y_\gamma &= \frac{1}{3}(y_a + y_b + y_c), \\ \kappa_\gamma &= \frac{1}{3}(x_a^2 + x_b^2 + x_c^2 + y_a^2 + y_b^2 + y_c^2). \end{aligned}$$

It can be observed from (13) that the *expected virtual distance* γ_e is served as a virtual measurement, compared with those true measurements r_ℓ for $\ell = 1, 2$, and 3. The noise matrix ψ in (10) can be obtained by

$$\psi = 2\, c\, \mathbf{B}\boldsymbol{n} + c^2\boldsymbol{n}^2, \tag{14}$$

where

$$\mathbf{B} = \mathrm{diag}\{\, \zeta_1, \quad \zeta_2, \quad \zeta_3, \quad \gamma\,\},$$
$$\boldsymbol{n} = [\, n_1 \quad n_2 \quad n_3 \quad n_\gamma/c\,]^T.$$

Based on the two-step LS scheme, an intermediate location estimate $\hat{z}$ after the first step can be obtained by

$$\hat{z} = \left[\, \hat{x}_i \quad \hat{y}_i \quad \hat{\beta}\,\right]^T = (\mathbf{H}^T\mathbf{\Psi^{-1}}\mathbf{H})^{-1}\mathbf{H}^T\mathbf{\Psi^{-1}}\mathbf{J}, \tag{15}$$

where $(\hat{x}_i, \hat{y}_i)$ is denoted as the intermediate location estimation of the MS after the first step of the algorithm. The weighting matrix $\mathbf{\Psi}$ is obtained by

$$\mathbf{\Psi} = \boldsymbol{E}[\psi\psi^T] = 4\, c^2\, \mathbf{BQB}. \tag{16}$$

It is noted that $\mathbf{\Psi}$ is obtained by neglecting the second term in (14). The matrix $\mathbf{Q}$ can be acquired as

$$\mathbf{Q} = \mathrm{diag}\{\, \sigma_{r_1}^2, \quad \sigma_{r_2}^2, \quad \sigma_{r_3}^2, \quad \sigma_{\gamma_e}^2/c^2\,\}.$$

It can be observed that $\mathbf{Q}$ represents the covariance matrix for both the TOA measurements and the *expected virtual distance*, where σ_{γ_e} corresponds to the standard deviation of γ_e. The final location estimation after the second step of the two-step LS algorithm can be obtained by [6]

$$\hat{\boldsymbol{x}} = [\, \hat{x} \quad \hat{y}\,]^T = \left[(\mathbf{H}'^T\mathbf{\Psi}'^{-1}\mathbf{H}')^{-1}\mathbf{H}'^T\mathbf{\Psi}'^{-1}\mathbf{J}'\right]^{1/2}, \tag{17}$$

where

$$\mathbf{H}' = \begin{bmatrix} 1 & 0 & 1 \\ 0 & 1 & 1 \end{bmatrix}^T \qquad \mathbf{J}' = \left[\, \hat{x}_i^2 \quad \hat{y}_i^2 \quad \hat{\beta}\,\right]^T,$$
$$\mathbf{\Psi}' = \boldsymbol{E}[\psi'\psi'^T] = 4\, \mathbf{B}'\, \mathrm{cov}(\hat{z})\, \mathbf{B}',$$
$$= 4\, \mathbf{B}'\, (\mathbf{H}^T\mathbf{\Psi}^{-1}\mathbf{H})^{-1}\, \mathbf{B}',$$
$$\mathbf{B}' = \mathrm{diag}\{\, \hat{x}_i, \quad \hat{y}_i, \quad 1/2\,\}.$$

3.3.2 Two TOA and One AOA Measurements

Due to the weak incoming signals or the shortage of signal sources (for example, at the rural area), there is great possibility that the MS may not be able to acquire enough signal sources from the environment, that is, only two TOA measurements are available from BS_1 and BS_2. In order to employ the proposed 2D GALE algorithm within this circumstance, an additional horizontal AOA measurement (that is, θ in (3)) from the home BS is adopted. As mentioned in the Third Generation Partnership Project (3GPP) standard [35], [36], each BS should be equipped with antenna arrays for adaptive beam steering in order to facilitate the AOA measurements. It is also noted that only the AOA measurement from the home BS is applied to avoid the signal degradation due to the near-far effect.

The geometric layout of the two TOA and the one AOA measurements is illustrated in Fig. 2. The proposed 2D GALE algorithm can be applied in this case with some

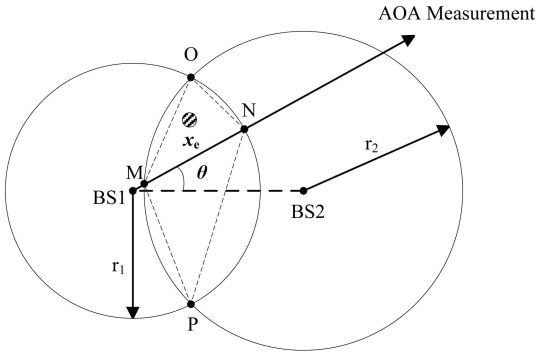

Fig. 2. The schematic diagram of the TOA/AOA-based location estimation for NLOS environments.

modifications from the three-TOA case. The region enclosed by points A, B, and C (as in Fig. 1) is replaced by the area defined from points M, N, O, and P. The intersecting points defined in (5) become $\boldsymbol{x}_\mu = \boldsymbol{x}_m$, $\boldsymbol{x}_n$, $\boldsymbol{x}_o$, and $\boldsymbol{x}_p$, where $\boldsymbol{x}_m = (x_m, y_m)$, $\boldsymbol{x}_n = (x_n, y_n)$, $\boldsymbol{x}_o = (x_o, y_o)$, and $\boldsymbol{x}_p = (x_p, y_p)$. The number of intersecting points m equals 4 in this case. The coordinates of the MS's expected position $\boldsymbol{x}_e = (x_e, y_e)$ is determined by (7) and (8) with $I_1 = \boldsymbol{x}_m$, $I_2 = \boldsymbol{x}_n$, $I_3 = \boldsymbol{x}_o$, and $I_4 = \boldsymbol{x}_p$. The standard deviations σ_1 and σ_2 are obtained from the TOA measurements, that is, $\sigma_1 = \sigma_{r_1}$ and $\sigma_2 = \sigma_{r_2}$, whereas σ_3 and σ_4 correspond to the same value, which is referred to as the signal variations coming from the horizontal AOA measurement θ. The selection of σ_3 and σ_4 is determined by $\sigma_3 = \sigma_4 = r_1 \cdot \sigma_\theta/c$, where σ_θ corresponds to the standard deviation of the measurement noise n_θ in (3). For instance, as the value of σ_3 (or σ_4) increases, the expected MS's position $\boldsymbol{x}_e$ should move away from the line that connects points M and N. The resulting location of $\boldsymbol{x}_e$ is expected to move toward either point O or P. The effect is coincident with the selection criterion of the weighting coefficient (that is, (8)), which results in larger values of w_3 and w_4. The distance effect d_k (as in (9)), which represents the relative distances between the intersecting points, is also considered for the determination of the *expected virtual distance* $\boldsymbol{x}_e$. The matrices associated in (10), (14), and (16) for the two TOA and one AOA measurements are listed as in Appendix.

3.4 The Proposed 3D Gale Algorithm

In this section, the proposed GALE algorithm is applied for the estimation of a 3D MS position. The design concept of the 3D GALE scheme can be extended from the 2D cases described in Section 3.3. The 3D geometric constraints from the cell layouts are adopted within the problem formulation of the two-step LS method. The following two cases are taken into account based on different scenarios.

3.4.1 Four TOA Measurements

Four BSs (that is, BS_1, BS_2, BS_3, and BS_4) associated with four TOA measurements are required for the estimation of a 3D MS's position. As illustrated in Fig. 3, every three of the four TOA measurements will form an enclosed rugbylike region with the existence of NLOS errors. The three TOA measurements will intersect at two points and the remainder, that is, the fourth TOA measurement, will decide which

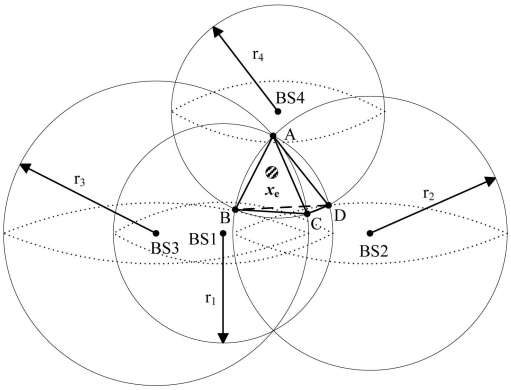

Fig. 3. The schematic diagram of the TOA-based location estimation for NLOS environments.

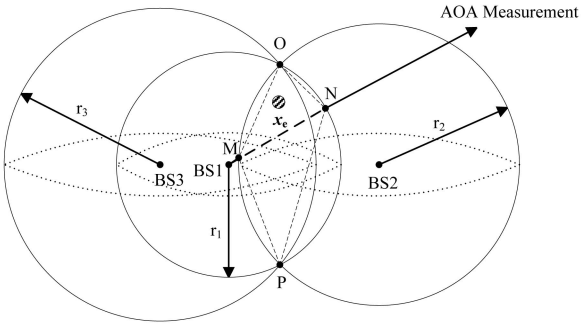

Fig. 4. The schematic diagram of the TOA/AOA-based location estimation for NLOS environments.

one of the intersecting points will be chosen. These selected points (that is, points A, B, C, and D in Fig. 3) will then be adopted within the 3D GALE algorithm. These four points will bring about an overlap region in which the expected position of the MS should be located. Similarly, the parameter $\boldsymbol{x}_\mu$, as defined in (5), becomes $\boldsymbol{x}_a = (x_a, y_a, z_a)$, $\boldsymbol{x}_b = (x_b, y_b, z_b)$, $\boldsymbol{x}_c = (x_c, y_c, z_c)$, and $\boldsymbol{x}_d = (x_d, y_d, z_d)$. The expected position of the MS $\boldsymbol{x}_e = (x_e, y_e, z_e)$ is determined with respect to points A, B, C, and D according to (7) and (8) with $I_1 = \boldsymbol{x}_a$, $I_2 = \boldsymbol{x}_b$, $I_3 = \boldsymbol{x}_c$, and $I_4 = \boldsymbol{x}_d$. For the determination of the weighting coefficients w_k, standard deviations σ_1, σ_2, σ_3, and σ_4 are obtained from the TOA measurements, that is, $\sigma_1 = \sigma_{r_1}$, $\sigma_2 = \sigma_{r_2}$, $\sigma_3 = \sigma_{r_3}$, and $\sigma_4 = \sigma_{r_4}$. Moreover, the state vector $\boldsymbol{z}$ (as in (11)) is enlarged to incorporate the z direction of the MS's position, that is, $\boldsymbol{z} = [x \quad y \quad z \quad \beta]^T$. The corresponding matrices are listed in Appendix B. Therefore, the GALE algorithm can be applied to solve for the 3D location estimation problem.

3.4.2 Three TOA and One AOA Measurements

With the shortage of incoming signals (that is, only three TOA measurements) from the BSs, the additional AOA measurement from the home BS can be adopted for the estimation of a 3D MS's location. As illustrated in Fig. 4, the three TOA measurements form a rugbylike region with two endpoints, O and P. The AOA measurement from the BS_1 will intersect the region at two points, M and N. The region enclosed by these four points will be utilized as the constrained area for the exploitation of the 3D GALE scheme. Similar to Section 3.3.2, the intersecting points defined in (5) can also be obtained by $\boldsymbol{x}_\mu = \boldsymbol{x}_m$, $\boldsymbol{x}_n$, $\boldsymbol{x}_o$, and $\boldsymbol{x}_p$, where $\boldsymbol{x}_m = (x_m, y_m, z_m)$, $\boldsymbol{x}_n = (x_n, y_n, z_n)$, $\boldsymbol{x}_o = (x_o, y_o, z_o)$, and $\boldsymbol{x}_p = (x_p, y_p, z_p)$. The MS's expected position $\boldsymbol{x}_e = (x_e, y_e, z_e)$ can therefore be determined based on (7) and (8).

Both σ_1 and σ_2 are obtained from the average standard deviations of the two TOA measurements where the intersecting point is not located, that is, if point M is located on the spherical surface created from the TOA measurement with radius r_3, σ_1 will be equal to the average of the standard deviations of measurements r_1 and r_2, that is, $\sigma_1 = (\sigma_{r_1} + \sigma_{r_2})/2$. This indicates that the weighting coefficient w_1 will be influenced by the combined effect from the standard deviations of the r_1 and r_2 measurements, that is, σ_{r_1} and σ_{r_2}. The standard deviations σ_3 and σ_4 correspond to the same value, which indicate the average value of the signal variations coming from both the horizontal and the vertical AOA measurements (that is, θ and ϕ). The selection of σ_3 and σ_4 is determined by $\sigma_3 = \sigma_4 = r_1 \cdot (\sigma_\theta + \sigma_\phi)/2c$, where σ_θ and σ_ϕ correspond to the standard deviations of the measurement noises n_θ and n_ϕ in (3) and (4). As the value of σ_3 increases, the expected MS's position $\boldsymbol{x}_e$ should move away from the line that connects points M and N. On the other hand, the weighting coefficients w_k are also affected by the distance effect d_k (as in (9)), which considers the relative capability of the expected MS's position to approach these four endpoints. The matrices associated in (10), (14), and (16) can be found in Appendix C. In the next section, the performance of both the proposed 2D and 3D GALE algorithms under different cases will be evaluated and compared via simulations.

4 Performance Evaluation

Simulations are performed to show the effectiveness of the proposed 2D and 3D GALE schemes under different scenarios. The noise models and the computation of CRLB are illustrated in Sections 4.1 and 4.2. The simulation parameters are listed in Section 4.3. The performance comparison between the proposed GALE algorithm and other existing location estimation schemes are conducted in Section 4.4.

4.1 The Noise Models

Different noise models [31], [33], [34], [37], [38] for the TOA and the AOA measurements are considered in the simulations. It is noticed that the statistical models suggested from the previous studies are primarily based on extensive field experiments and observations. The model for the measurement noise of the TOA signal is assumed to be Gaussian distributed with its probability density function defined as

$$f_{n_{\ell,m}}(\upsilon) = f_{n_m}(\upsilon) = \frac{1}{\sqrt{2\pi}\,\sigma_m} \exp\left(-\frac{\upsilon^2}{2\sigma_m^2}\right), \tag{18}$$

where all the TOA measurements are considered to share the same distribution. The mean value n_m is assumed to be zero, whereas the standard deviation $\sigma_m = 10\ m$. It is noted that the mean of the measurement noise is chosen to be zero since the value is considered as the noiseless distance ζ_ℓ. On the other hand, an exponential distribution $f_{n_{\ell,nl}}(\upsilon)$ is assumed for the NLOS noise model of the TOA measurements [37]:

$$f_{n_{\ell,nl}}(\upsilon)=\begin{cases}\frac{1}{\lambda_\ell}\exp\left(-\frac{\upsilon}{\lambda_\ell}\right) & \upsilon>0\\ 0 & \upsilon\le 0,\end{cases} \tag{19}$$

where $\lambda_\ell = c\cdot\tau_\ell = c\cdot\tau_m\zeta_\ell^{\varepsilon}\rho$ for $\ell = 1, 2, 3$, and 4. τ_ℓ is the root-mean-square (RMS) delay spread from the ℓth BS to the MS, and τ_m is the median value of τ_ℓ, whose value depends on various environments. The performance of the location schemes will be evaluated under different τ_m values in Section 4.2. ε is the path loss exponent, which is assumed to be 0.5, and the factor for shadow fading ρ is set to 1 in the simulations. It is noted that parameter λ_ℓ also depends on the relative distance between the MS and BS_ℓ, that is, ζ_ℓ. Moreover, the probability density functions of the noise models for the horizontal AOA measurement ($f_{n_\theta}(\upsilon)$) and the vertical AOA measurement ($f_{n_\phi}(\upsilon)$) are assumed to be uniformly distributed [38]:

$$f_{n_\theta}(\upsilon)=f_{n_\phi}(\upsilon)=\begin{cases}\frac{1}{2\lambda_a} & -\lambda_a\le\upsilon\le\lambda_a\\ 0 & \upsilon<-\lambda_a \text{ or } \upsilon>\lambda_a,\end{cases} \tag{20}$$

where λ_a is chosen to be 10, which indicates that the measurement noise associated with the AOA signal varies between -10^o and 10^o in both the horizontal and the vertical directions. It is noticed that the parameters for the noise models listed in this section primarily fulfill the environment while the MS is located within the suburban area.

4.2 Computation of the Cramér-Rao Lower Bound (CRLB)

In this section, the derivation of the Cramér-Rao Lower Bound (CRLB) is acquired based on the noise models described in Section 4.1. CRLB is a lower bound on the variance of a statistical estimator [39]. It has been investigated to provide a lower bound for the variance of the location estimators based on Gaussian-distributed measurement inputs [40]. However, the CRLB based on different noise models has not been developed for location estimation. In order to provide a variance lower bound for the location estimation algorithms (that is, the GALE, the two-step LS, and the LLOP schemes), the CRLB based on various distributions of measurement inputs is derived in this section. As was indicated in (1), the measured distance from the TOA signal r_ℓ consists of the noiseless distance ζ_ℓ, the measurement noise $n_{\ell,m}$, and the NLOS error $n_{\ell,nl}$. The probability density function for the combined noiseless distance ζ_ℓ and the measurement noise $n_{\ell,m}$ can be obtained by

$$f_{\zeta_\ell+n_{\ell,m}}(\upsilon)=\frac{1}{\sqrt{2\pi}\,\sigma_m}\exp\left(-\frac{(\upsilon-\zeta_\ell)^2}{2\sigma_m^2}\right), \tag{21}$$

which corresponds to a Gaussian-distributed model with a mean equal to ζ_ℓ and σ_m as the standard deviation. Therefore, the probability density function of the measured distance from the TOA signal r_ℓ is considered as the combination of a Gaussian-distributed signal (that is, $f_{\zeta_\ell+n_{\ell,m}}(\upsilon)$) and an exponentially distributed signal (that is, $f_{n_{\ell,nl}}(\upsilon)$). It can be acquired by convoluting (19) and (21) as

$$\begin{aligned}f_{r_\ell}(\upsilon)&=\int_{-\infty}^{\upsilon} f_{\zeta_\ell+n_{\ell,m}}(\omega)\,f_{n_{\ell,nl}}(\upsilon-\omega)\,d\omega\\ &=\frac{1}{\lambda_\ell}\exp\left(-\frac{\upsilon-\zeta_\ell}{\lambda_\ell}+\frac{\sigma_m^2}{2\lambda_\ell^2}\right)\mathbf{\Phi}\left(\frac{\upsilon-\zeta_\ell}{\sigma_m}-\frac{\sigma_m}{\lambda_\ell}\right),\end{aligned} \tag{22}$$

where $\mathbf{\Phi}(\upsilon)=\int_{-\infty}^{\upsilon}\frac{1}{\sqrt{2\pi}}\exp(-\frac{\omega^2}{2})d\omega$. Moreover, the probability density functions for the AOA measurements $f_\theta(\upsilon)$ and $f_\phi(\upsilon)$ can be obtained by (from (3), (4), and (20)):

$$f_\theta(\upsilon)=\begin{cases}\frac{1}{2\lambda_a} & -\lambda_a+\theta_t\le\upsilon\le\lambda_a+\theta_t\\ 0 & \text{otherwise,}\end{cases} \tag{23}$$

$$f_\phi(\upsilon)=\begin{cases}\frac{1}{2\lambda_a} & -\lambda_a+\phi_t\le\upsilon\le\lambda_a+\phi_t\\ 0 & \text{otherwise.}\end{cases} \tag{24}$$

It is assumed that all the measurements from different BSs are independent, including both the TOA and the AOA signals. By considering the case with TOA/AOA measurements for the 3D location estimation, the joint probability density function $f_{\boldsymbol{r},\boldsymbol{\theta}}(\boldsymbol{\upsilon};\boldsymbol{z}_p)$ with respect to the variable $\boldsymbol{z}_p=[\boldsymbol{x},\theta_t,\phi_t]^T=[x,y,z,\theta_t,\phi_t]^T$ can be obtained by

$$\begin{aligned}f_{\boldsymbol{r},\boldsymbol{\theta}}(\boldsymbol{\upsilon};\boldsymbol{z}_p)&=\prod_{\ell=1}^{N} f_{r_\ell}(\upsilon_\ell;\boldsymbol{x})\cdot f_\theta(\upsilon_\theta;\boldsymbol{x},\theta_t)\cdot f_\phi(\upsilon_\phi;\boldsymbol{x},\phi_t)\\ &=\frac{1}{4\lambda_a^2}\prod_{\ell=1}^{N}\frac{1}{\lambda_\ell}\exp\left(-\frac{\upsilon_\ell-\zeta_\ell}{\lambda_\ell}+\frac{\sigma_m^2}{2\lambda_\ell^2}\right)\cdot\mathbf{\Phi}\left(\frac{\upsilon_\ell-\zeta_\ell}{\sigma_m}-\frac{\sigma_m}{\lambda_\ell}\right),\end{aligned} \tag{25}$$

where $\boldsymbol{r}=[r_1,\ldots,r_N]^T$, $\boldsymbol{\theta}=[\theta,\phi]^T$, and $\boldsymbol{\upsilon}=[\upsilon_1,\ldots,\upsilon_N,\upsilon_\theta,\upsilon_\phi]^T$. From (25), the natural logarithm of $f_{\boldsymbol{r},\boldsymbol{\theta}}(\boldsymbol{\upsilon};\boldsymbol{z}_p)$ can be expressed as

$$\begin{aligned}\ln f_{\boldsymbol{r},\boldsymbol{\theta}}(\boldsymbol{\upsilon};\boldsymbol{z}_p)=&-\ln(4\lambda_a^2)+\sum_{\ell=1}^{N}\left[\ln\mathbf{\Phi}\left(\frac{\upsilon_\ell-\zeta_\ell}{\sigma_m}-\frac{\sigma_m}{\lambda_\ell}\right)\right.\\ &\left.-\ln\lambda_\ell+\left(-\frac{\upsilon_\ell-\zeta_\ell}{\lambda_\ell}+\frac{\sigma_m^2}{2\lambda_\ell^2}\right)\right].\end{aligned} \tag{26}$$

The partial derivative of $\ln f_{\boldsymbol{r},\boldsymbol{\theta}}(\boldsymbol{\upsilon};\boldsymbol{z}_p)$ with respect to $\boldsymbol{z}_p$ can be obtained by

$$\begin{aligned}&\frac{\partial}{\partial\boldsymbol{z}_p}\ln f_{\boldsymbol{r},\boldsymbol{\theta}}(\boldsymbol{\upsilon};\boldsymbol{z}_p)=\\ &\sum_{\ell=1}^{N}\left[\frac{1}{\lambda_\ell}\frac{\partial\zeta_\ell}{\partial\boldsymbol{z}_p}+\mathbf{\Phi}^{-1}\left(\frac{\upsilon_\ell-\zeta_\ell}{\sigma_m}-\frac{\sigma_m}{\lambda_\ell}\right)\cdot\frac{\partial}{\partial\boldsymbol{z}_p}\mathbf{\Phi}\left(\frac{\upsilon_\ell-\zeta_\ell}{\sigma_m}-\frac{\sigma_m}{\lambda_\ell}\right)\right],\end{aligned} \tag{27}$$

where

$$\frac{\partial\zeta_\ell}{\partial\boldsymbol{z}_p}=\frac{1}{\zeta_\ell}[(x-x_\ell)\ \ (y-y_\ell)\ \ (z-z_\ell)]^T, \tag{28}$$

$$\begin{aligned}\frac{\partial}{\partial\boldsymbol{z}_p}\mathbf{\Phi}\left(\frac{\upsilon_\ell-\zeta_\ell}{\sigma_m}-\frac{\sigma_m}{\lambda_\ell}\right)=&\frac{-\exp\left[\frac{-(\sigma_m^2+\lambda_\ell\zeta_\ell-\lambda_\ell\upsilon_\ell)^2}{2\lambda_\ell^2\sigma_m^2}\right]}{\sqrt{2\pi}\zeta_\ell\,\sigma_m}\cdot\\ &[(x-x_\ell)\ \ (y-y_\ell)\ \ (z-z_\ell)]^T.\end{aligned} \tag{29}$$

By adopting (27)-(29), the CRLB (Υ) based on various types of measurement signals can be obtained:

$$\Upsilon=\left\{E\left[\frac{\partial}{\partial\boldsymbol{z}_p}\ln f_{\boldsymbol{r},\boldsymbol{\theta}}(\boldsymbol{\upsilon};\boldsymbol{z}_p)\cdot\left(\frac{\partial}{\partial\boldsymbol{z}_p}\ln f_{\boldsymbol{r},\boldsymbol{\theta}}(\boldsymbol{\upsilon};\boldsymbol{z}_p)\right)^T\right]_{\boldsymbol{z}_p=\boldsymbol{z}_p^0}\right\}^{-1}, \tag{30}$$

where $\boldsymbol{z}_p^0$ denotes the true values in the $\boldsymbol{z}_p$ vector, which are substituted into (30) for the computation of Υ. It is noted

TABLE 1
Performance Comparison between the Location Estimation Algorithms for the 2D Case with Three TOA Measurements (Estimation Error (m))

	10%	20%	30%	40%	50%	60%	70%	80%	90%	100%
GALE	27.36	67.28	83.59	103.72	138.07	159.44	184.07	265.12	309.39	470.43
Two-Step LS	53.70	94.72	133.98	147.08	172.22	199.42	252.91	280.15	377.03	588.79
LLOP	35.27	68.74	107.61	132.00	166.74	185.78	229.75	275.37	361.44	520.90
RSA	33.15	68.24	105.11	131.13	165.07	181.57	226.14	272.63	356.16	514.93

TABLE 2
Performance Comparison between the Location Estimation Algorithms for the 2D Case with Two TOA and One AOA Measurements (Estimation Error (m))

	10%	20%	30%	40%	50%	60%	70%	80%	90%	100%
GALE	16.07	25.31	31.80	39.09	48.10	56.83	66.68	79.53	104.12	780.58
Two-Step LS	17.24	25.76	33.49	41.70	51.93	61.42	69.79	86.16	118.06	909.04
HLOP	26.08	42.94	56.68	70.30	87.23	103	122.58	156.07	212.69	790.71

TABLE 3
Performance Comparison between the Location Estimation Algorithms for the 3D Case with Four TOA Measurements (Estimation Error (m))

	10%	20%	30%	40%	50%	60%	70%	80%	90%	100%
GALE	118.5	159.87	185.44	210.05	221.05	246.07	274.85	351.55	506.87	976.5
Two-Step LS	194.38	208.23	245	291.73	383.01	466.87	562.76	603.8	713.81	1148.7
LLOP	191.85	380.36	574.43	876.91	1129.6	1667	1910	2313.6	3063.3	6720

TABLE 4
Performance Comparison between the Location Estimation Algorithms for the 3D Case with Three TOA and One AOA Measurements (Estimation Error (m))

	10%	20%	30%	40%	50%	60%	70%	80%	90%	100%
GALE	13.95	18.79	23.23	28.58	34.51	42.23	54.25	72.75	107.55	358.24
Two-Step LS	14.12	19.52	23.83	30.24	36.48	44.49	58.56	79.69	125.96	404.2
HLOP	28.68	41.89	55.70	70.50	87.08	108.22	135.85	186.4	297.8	3172.41

that (30) represents the CRLB with the TOA/AOA measurements for 3D location estimation. The CRLB for other scenarios (for example, the TOA/AOA measurements for 2D location estimation or the TOA measurements for 3D location estimation) can easily be obtained by neglecting several terms in (28) and (29). In the simulations, the CRLBs for the various cases will be utilized to provide the lower bounds for the estimation variances while comparing different location estimation schemes.

4.3 Simulation Parameters

Each case is conducted with 1,000 runs of simulations. The simulation parameters associated with the two cases in the 2D scenarios (as described in Section 3.3) are listed as follows:

1. *Three TOA case*. The home BS, that is, BS_1, is located at (0, 0) in meters, whereas the positions of the other two BSs, BS_2 and BS_3, are located at $(1{,}000, 1{,}000\sqrt{3})$ and $(-1{,}000, 1{,}000\sqrt{3})$ in meters. The true position of the MS is assumed to be at $(600 \cdot U_m - 300, 600 \cdot U_m - 300)$ in meters, where U_m represents a uniform distribution function within the interval [0 1]. As a result, the MS is selected to be uniformly distributed around the neighborhood of the home BS, that is, BS_1.
2. *Two TOA with one AOA case*. The signal from BS_3 is assumed unavailable in this case. The MS can only receive the signals from both BS_1 and BS_2 with their coordinates as indicated in the first case. The true position of the MS is located at $(500 \cdot U_m, 500 \cdot U_m)$ in meters.

The parameters for the 3D cases (as in Section 3.4) are listed as follows:

1. *Four TOA case*. The home BS, that is, BS_1, is located at (0, 0, 260) in meters, whereas the positions of the other three BSs, BS_2, BS_3, and BS_4, are located at $(250\sqrt{3}, 250\sqrt{3}, 240)$, $(-250\sqrt{3}, 250\sqrt{3}, 180)$, and (500, 0, 290) in meters. The true position of the MS is assumed to be at $(160 \cdot U_m, 160 \cdot U_m, 220 - 50 \cdot U_m)$ in meters in this case.
2. *Three TOA with one AOA case*. The signal from BS_4 is assumed unavailable in this case. The MS can only receive the signals from BS_1, BS_2, and BS_3 with their coordinates as indicated in the four TOA case. The true position of the MS is located at $(160 \cdot U_m, 160 \cdot U_m, 220 - 50 \cdot U_m)$ in meters.

4.4 Simulation Results

Tables 1, 2, 3, and 4 and Figs. 5, 6, 7, 8, 9, 10, 11, 12, 13, 14, and 15 show the performance evaluation of the proposed

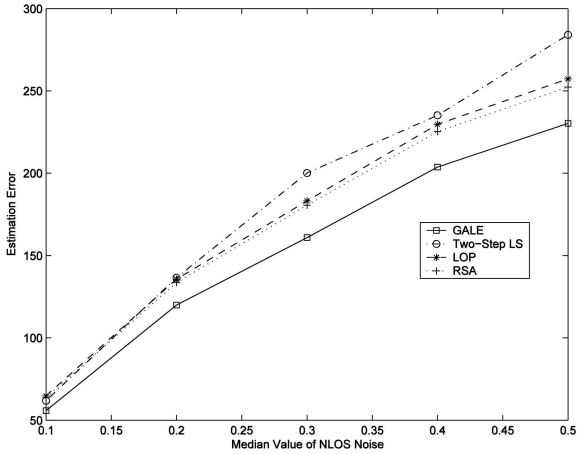

Fig. 5. Performance comparison between the location estimation algorithms for the 2D case with three TOA measurements: average estimation error versus NLOS noises.

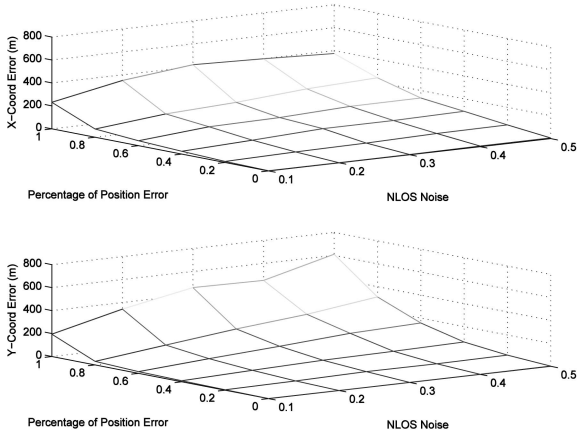

Fig. 6. Location estimation using the GALE algorithm for the 2D case with three TOA measurements: (top plot) x-direction error (m) versus percentage of position errors and the NLOS noises; (bottom plot) y-direction error (m) versus percentage of position errors and the NLOS noises.

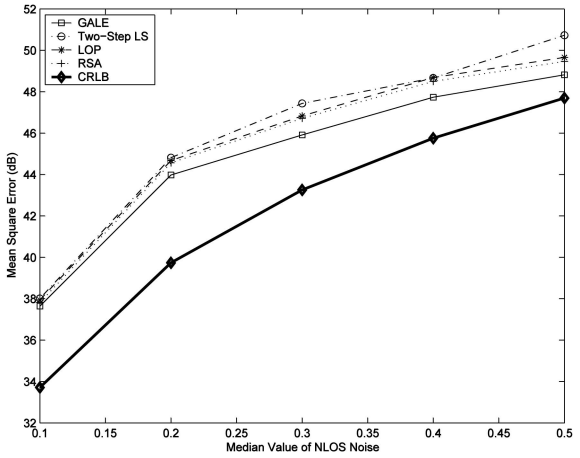

Fig. 7. Performance comparison between the location estimation algorithms for the 2D case with three TOA measurements: MSE versus NLOS noises (with 50 percent position error).

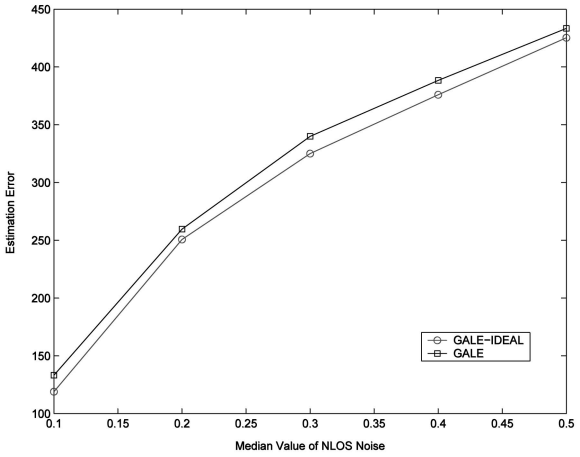

Fig. 8. Sensitivity analysis of the GALE algorithm for the 2D case with three TOA measurements: average estimation error versus NLOS noises (with 95 percent position error).

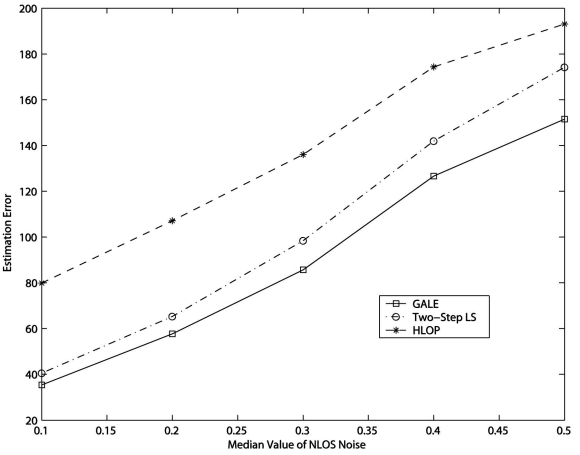

Fig. 9. Performance comparison between the location estimation algorithms for the two TOA and one AOA case: average estimation error versus NLOS noises.

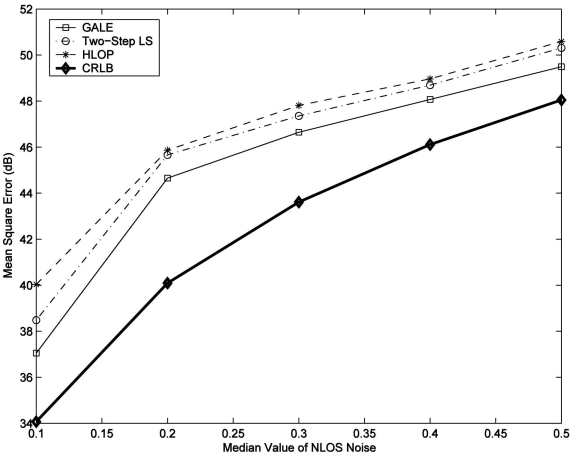

Fig. 10. Performance comparison between the location estimation algorithms for the two TOA and one AOA Case: MSE versus NLOS noises (with 50 percent position error).

GALE algorithm. The GALE scheme is compared with the two-step LS, the LLOP, and the RSA techniques under different situations. It is noted that both the two-step LS algorithm [6] and the LLOP scheme [29] are adopted from the previous work for the 2D MS's location estimation. The 3D location estimation using these two schemes are derived

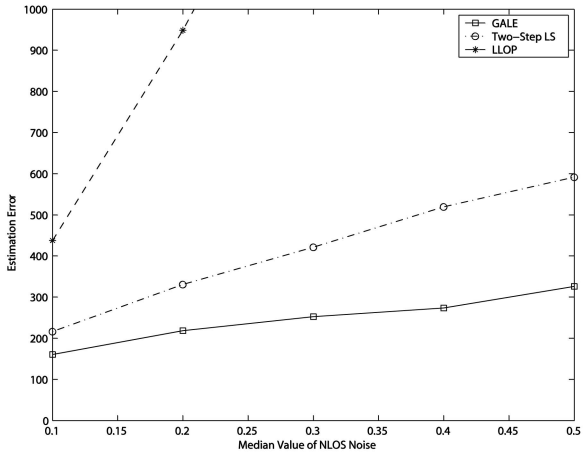

Fig. 11. Performance comparison between the location estimation algorithms for the 3D case with four TOA measurements: average estimation error versus NLOS noises.

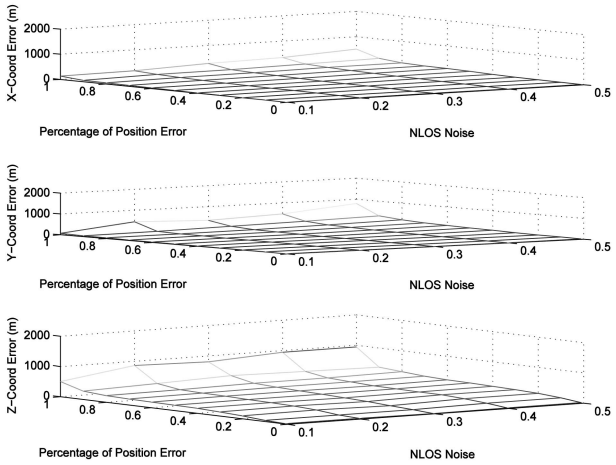

Fig. 12. Location estimation using the GALE algorithm for the 3D case with four TOA measurements: (top plot) x-direction error (m) versus percentage of position errors and the NLOS noises; (middle plot) y-direction error (m) versus percentage of position errors and the NLOS noises; (bottom plot) z-direction error (m) versus percentage of position errors and the NLOS noises.

and extended in this paper in order to demonstrate the performance comparison with the proposed 3D GALE algorithm. However, the RSA scheme [32] was originally formulated for the estimation of the 2D MS's location under three TOA measurements. Due to its intricate formulation and difficulty for extension, it will only be utilized for performance comparison for the 2D case with three TOA measurements.

4.4.1 Simulation Results for the 2D Cases

Table 1 and Figs. 5, 6, and 7 illustrate the performance comparison between the location estimation schemes for the 2D case with three TOA measurements. Table 1 illustrates the comparison between these schemes under different percentages of position errors, which is obtained by sorting the entire set of estimation errors according to their magnitudes. The enhanced 911 of the Federal Communications Commission (FCC) [1] defines the location accuracy requirements for both 67 percent and 95 percent of position errors for the network-based location systems. In order to provide a more comprehensive comparison, the complete set of the percentage of position errors is revealed in Table 1.

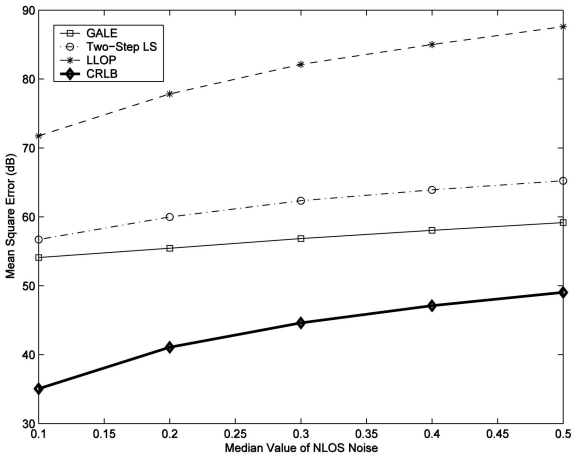

Fig. 13. Performance comparison between the location estimation algorithms for the 3D case with four TOA measurements: MSE versus NLOS noises (with 50 percent position error).

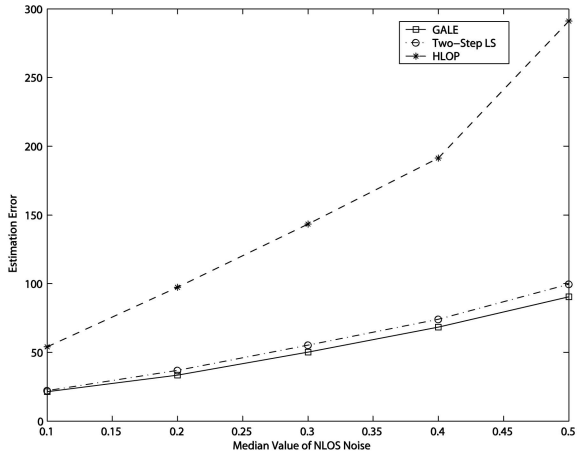

Fig. 14. Performance comparison between the location estimation algorithms for the three TOA and one AOA case: average estimation error versus NLOS noises.

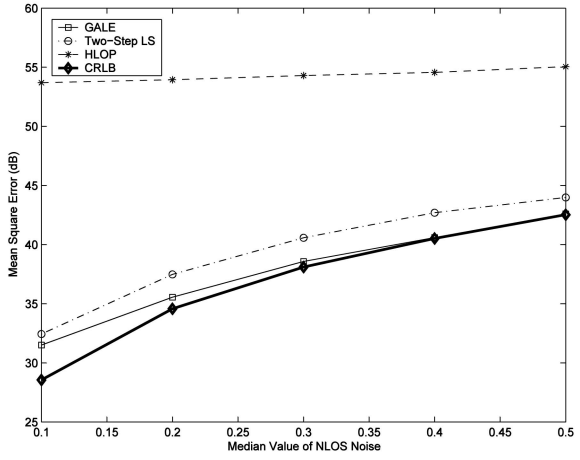

Fig. 15. Performance comparison between the location estimation algorithms for the three TOA and one AOA case: MSE versus NLOS noises (with 50 percent position error).

It can be seen in Table 1 that the proposed 2D GALE algorithm can achieve better estimation performance compared with the other three approaches. It is noted that the data are obtained under $\tau_m = 0.3\ \mu s$. The GALE scheme can outperform the RSA, the LLOP, and the two-step LS methods with around 47, 52, and 67 meters of estimation errors under 90 percent of position errors. The sudden increases in the percentage of position errors between 90 percent and 100 percent primarily resulted from the larger noises (combination of the NLOS and the measurement noises) due to the utilization of the probability models, that is, those data are considered to have the largest standard deviation from their noise models. It is also noticed that the estimation error of the MS's position is represented as $\Delta\hat{\boldsymbol{x}} = \|\hat{\boldsymbol{x}} - \boldsymbol{x}\|$, where $\hat{\boldsymbol{x}}$ represents the final location estimate from the location estimation algorithms.

Fig. 5 shows the comparison between these schemes under different NLOS errors. It represents the average position errors with variations on the τ_m values, that is, $\tau_m = 0.1, 0.2, 0.3, 0.4$, and $0.5\ \mu s$. As can be seen from the figure, the estimation errors are severely increased as the value of the NLOS noise is raised. It can be found that the GALE algorithm can still achieve better performance, especially with larger NLOS noises. The GALE approach can provide around $50\,m$ less in the estimation error compared to the two-step LS scheme and around 25 m less in comparison with the RSA and the LLOP methods (under $\tau_m = 0.5\ \mu s$). Fig. 6 shows the location estimation errors obtained from the GALE algorithm in both the x and y-directions, that is, $\Delta x = |\hat{x} - x|$ and $\Delta y = |\hat{y} - y|$. Both subplots are conducted under different percentages of position errors and NLOS noises. It can be observed that the estimation errors in both the x and y-directions follow similar trends and values under the various situations. Moreover, Fig. 7 shows the Mean Square Error (MSE) of location estimation versus different τ_m values. The results are obtained at a specific location of the MS (that is, $\boldsymbol{x} = (107, 241)$) due to the CRLB requirement in (30). It is noted that $\mathrm{MSE} = 10 \cdot \log[\frac{1}{N}\sum_1^N \|\hat{\boldsymbol{x}} - \boldsymbol{x}\|^2]$ in decibels, where N indicates the number of runs in the simulations. The four location estimation schemes are illustrated with the associated CRLB for three TOA measurements. It can be observed that the CRLB provides the lower bound for this scenario, which also increases as τ_m is augmented. The proposed GALE scheme can still offer the smallest MSE for location estimation compared with the other three algorithms.

In order to illustrate the feasibility of the proposed GALE algorithm, the sensitivity of the location estimation obtained from the GALE scheme is analyzed according to the initial estimate of the noise matrix ψ (as in (14)). As shown in Fig. 8, the simulation results for the GALE-IDEAL case is obtained by adopting the true values of 1) the weighting matrix $\mathbf{B} = \mathrm{diag}\{\zeta_1, \zeta_2, \zeta_3, \gamma\}$, where the elements in $\mathbf{B}$ are computed by assuming a known value of the MS's position, and 2) $\mathbf{n} = \{n_1, n_2, n_3, n_\gamma/c\}$, where the noise values are obtained directly from the noise models (as in (18) and (19)) for each simulation. On the other hand, the simulation results for the GALE scheme is acquired by considering the estimated value of $\mathbf{B}$ and $\mathbf{n}$ as $\hat{\mathbf{B}} = \mathrm{diag}\{r_1, r_2, r_3, \gamma_e\}$ and $\hat{\mathbf{n}} = \{\sigma_{r_1}, \sigma_{r_2}, \sigma_{r_3}, \sigma_{\gamma_e}/c\}$, where the elements in $\hat{\mathbf{B}}$ and $\hat{\mathbf{n}}$ are computed from the measurement inputs. It can be observed in Fig. 8 that the deviations between the GALE scheme and the GALE-IDEAL line are considered not significant, that is, around 8 to 10 m differences of estimation error under the various values of τ_m.

Table 2 and Figs. 9 and 10 illustrate the performance comparison for the 2D case with two TOA and one AOA measurements. It is noted that the Hybrid Line-Of-Position (HLOP) scheme [30], which combines both the TOA and the AOA measurements, is utilized for comparison purposes. It can also be seen in Table 2 that the proposed 2D GALE algorithm can obtain better estimation performance compared with the other two methods under different percentages of position errors (with $\tau_m = 0.3\ \mu s$). Compared with the two-step LS method and the HLOP scheme, around 7 m and 76 m fewer estimation errors under 80 percent of average position errors can be achieved using the GALE scheme. Fig. 9 shows the average estimation errors from these three algorithms under different NLOS environments. It can also be seen that the proposed 2D GALE approach can provide around 25 m and 45 m fewer estimation errors in comparison with the two-step LS and the HLOP schemes (under $\tau_m = 0.5\ \mu s$). The MSE for location estimation under different τ_m is illustrated in Fig. 10, which is conducted with $\boldsymbol{x} = (358, 60)$. The proposed GALE scheme provides around 1 dB and 2 dB less MSE compared with the two-step LS and the HLOP methods.

4.4.2 Simulation Results for the 3D Cases

Table 3 and Figs. 11 and 13 illustrate the performance comparison between the location estimation schemes for the 3D case with four TOA measurements. Table 3 shows the estimation errors obtained from the three schemes under different percentages of position errors (at $\tau_m = 0.3\ \mu s$). It can be seen in Table 3 that the proposed 3D GALE algorithm can acquire much better performance compared with the other two schemes. The GALE scheme outperforms the two-step LS and the LLOP methods with around 252 m and 1,962 m of estimation errors, respectively, under 80 percent of average position errors. Fig. 11 shows the average position errors by comparing the three schemes under different NLOS noises. It is perceived that the proposed 3D GALE algorithm can achieve better performance with around 280 m less estimation error compared with the two-step LS method (under $\tau_m = 0.5\ \mu s$).

Fig. 12 shows the location estimation errors acquired from the GALE algorithm in the x, y, and z-coordinates (that is, $\Delta x = |\hat{x} - x|$, $\Delta y = |\hat{y} - y|$, and $\Delta z = |\hat{z} - z|$) for the 3D case with four TOA measurements. It can be found that excessive numbers of estimation errors have been observed in the z-direction compared with the other two directions in most situations. The reason is due to the different orders of magnitude between the vertical and the horizontal distances within the cell layouts [41]. The relative horizontal distances between the MS and the BSs can reach around the range of kilometers, whereas the MS's heights obtained

from the z-directions usually ranged in meters. It has also been experimented and validated in our simulations that the z-direction position errors of the MS can be reduced as the horizontal relative distances between the BSs are decreased (that is, lowered to the range of meter scale). Based on the above findings, it can be suggested that the 3D GALE algorithm is especially feasible to be adopted in the scenarios of microcell layouts.

Fig. 13 shows the MSE of the three schemes and the associated CRLB under four TOA measurements (at $\boldsymbol{x} = (108, 103, 21)$). It can be observed that the GALE algorithm outperforms the two-step LS and the LLOP schemes with 5 and 30 dB fewer MSE errors under $\tau_m = 0.5\ \mu s$. Compared with the 2D cases, it is observed in Table 3 and Figs. 11 and 13 that the effectiveness of the proposed GALE scheme can be demonstrated especially in the 3D case. The 3D GALE algorithm can still provide reasonable precision for location estimation, whereas the other two schemes result in excessive position errors. Moreover, it can be found that the LLOP scheme within the 3D scenarios suffers from severe estimation errors, which does not happen in the 2D cases. The reasons can be explained by observing the geometric intersection from the LLOP algorithm. In the 3D case, the four planes derived from the four TOA measurements may not intersect with each other for location estimation, whereas the definite intersections can be obtained between linear lines for the 2D case. As a result, the LLOP scheme within the 3D scenarios will induce poor accuracy for the location estimation of the MS.

Table 4 and Figs. 14 and 15 illustrate the performance comparison for the 3D case with three TOA and one AOA measurements. As shown in Table 4 (with $\tau_m = 0.3$), the GALE algorithm can obtain better location estimation accuracy compared with the other schemes. Under 80 percent of position errors, the GALE algorithm can achieve around 7 and 114 m fewer estimation errors compared with the two-step LS and the HLOP methods. Fig. 14 shows the comparison of the average estimation errors between these three schemes under different NLOS noises. Compared with the two-step LS and the HLOP schemes, the GALE approach can provide around 10 m and 200 m fewer estimation errors, respectively, in the position error under $\tau_m = 0.5\ \mu s$. Fig. 15 illustrates the MSE of the location estimate under different NLOS noises (at $\boldsymbol{x} = (50, 75, 21)$). The proposed GALE scheme can achieve better performance compared with the other two methods.

The merits of considering the geometric constraints within the formulation of the proposed GALE scheme can be observed from these simulation results. A feasible location estimate of the MS, both in the 2D and 3D scenarios, can be acquired within the efficient GALE scheme proposed.

5 Conclusion

An efficient GALE algorithm is proposed in this paper. The proposed GALE algorithm can be utilized for the estimation of either the 2D or the 3D position of the MS. The GALE scheme enhances the conventional two-step LS algorithm by imposing additional geometric constraints within its formulation. By using the proposed GALE algorithm, the computational efficiency acquired from the two-step LS method is preserved. Moreover, higher location estimation accuracy for the MS is also achieved, especially under NLOS environments. Different types of geometric layouts between the MS and its associated BSs are considered both in the design of the GALE algorithm and in the performance comparison. It is shown in the simulation results that the proposed GALE algorithm provides a better position location estimate compared with other existing methods.

Appendix A

A.1 Matrices for the 2D GALE Algorithm with Two TOA and One AOA Measurements

For the case of two TOA and one AOA measurements, matrices $\mathbf{H}$ and $\mathbf{J}$ in (10) are reformulated as

$$\mathbf{H} = \begin{bmatrix} \mathbf{H}_{TOA}^{2\times 3} \\ \mathbf{H}_{AOA}^{1\times 3} \\ \mathbf{H}_{\gamma}^{1\times 3} \end{bmatrix} = \begin{bmatrix} -2x_1 & -2y_1 & 1 \\ -2x_2 & -2y_2 & 1 \\ -\sin\theta & \cos\theta & 0 \\ -2x_\gamma & -2y_\gamma & 1 \end{bmatrix}, \tag{31}$$

$$\mathbf{J} = \begin{bmatrix} \mathbf{J}_{TOA}^{2\times 1} \\ \mathbf{J}_{AOA}^{1\times 1} \\ \mathbf{J}_{\gamma}^{1\times 1} \end{bmatrix} = \begin{bmatrix} r_1^2 - \kappa_1 \\ r_2^2 - \kappa_2 \\ -x_1\sin\theta + y_1\cos\theta \\ \gamma_e^2 - \kappa_\gamma \end{bmatrix}. \tag{32}$$

Matrices $\mathbf{B}$, $\mathbf{n}$, and $\mathbf{Q}$ associated with the noise matrix $\mathbf{\Psi}$ (as in (14) and (16)) can be obtained by

$$\begin{aligned} \mathbf{B} &= \mathrm{diag}\{\, \zeta_1, \quad \zeta_2, \quad \zeta_1, \quad \gamma \,\}, \\ \mathbf{n} &= [\, n_1 \quad n_2 \quad n_\theta \quad n_\gamma/c \,]^T, \\ \mathbf{Q} &= \mathrm{diag}\{\, \sigma_{r_1}^2, \quad \sigma_{r_2}^2, \quad \sigma_\theta^2, \quad \sigma_{\gamma_e}^2/c^2 \,\}. \end{aligned}$$

It is noted that value in the third diagonal term within matrix $\mathbf{B}$, that is, the element ζ_1, can be obtained as in [28] based on the geometric approximation of the AOA measurement.

A.2 Matrices for the 3D GALE Algorithm with Four TOA Measurements

For the case of four TOA measurements, the corresponding matrices, $\mathbf{H}$ and $\mathbf{J}$, in (10) should be modified to incorporate the additional z-dimension for location estimation as follows:

$$\mathbf{H} = \begin{bmatrix} \mathbf{H}_{TOA}^{4\times 4} \\ \mathbf{H}_{\gamma}^{1\times 4} \end{bmatrix} = \begin{bmatrix} -2x_1 & -2y_1 & -2z_1 & 1 \\ -2x_2 & -2y_2 & -2z_2 & 1 \\ -2x_3 & -2y_3 & -2z_3 & 1 \\ -2x_4 & -2y_4 & -2z_4 & 1 \\ -2x_\gamma & -2y_\gamma & -2z_\gamma & 1 \end{bmatrix}, \tag{33}$$

$$\mathbf{J} = \begin{bmatrix} \mathbf{J}_{TOA}^{4\times 1} \\ \mathbf{J}_{\gamma}^{1\times 1} \end{bmatrix} = \begin{bmatrix} r_1^2 - \kappa_1 \\ r_2^2 - \kappa_2 \\ r_3^2 - \kappa_3 \\ r_4^2 - \kappa_4 \\ \gamma_e^2 - \kappa_\gamma \end{bmatrix}, \tag{34}$$

where the coefficients within the matrices can be obtained by

$$
\begin{aligned}
\beta &= x^2 + y^2 + z^2, \\
\kappa_\ell &= x_\ell^2 + y_\ell^2 + z_\ell^2 \quad \text{for } \ell = 1,2,3,4, \\
x_\gamma &= \frac{1}{4}(x_a + x_b + x_c + x_d), \\
y_\gamma &= \frac{1}{4}(y_a + y_b + y_c + y_d), \\
z_\gamma &= \frac{1}{4}(z_a + z_b + z_c + z_d), \\
\kappa_\gamma &= \frac{1}{4}\big(x_a^2 + x_b^2 + x_c^2 + x_d^2 + y_a^2 + y_b^2 + y_c^2 + y_d^2 \\
&\quad + z_a^2 + z_b^2 + z_c^2 + z_d^2\big).
\end{aligned}
$$

Matrices $\mathbf{B}$, $\mathbf{n}$, and $\mathbf{Q}$ associated with the noise matrix ψ, as in (14) and (16), are adjusted as

$$
\begin{aligned}
\mathbf{B} &= \operatorname{diag}\{\, \zeta_1, \quad \zeta_2, \quad \zeta_3, \quad \zeta_4, \quad \gamma \,\}, \\
\mathbf{n} &= [\, n_1 \quad n_2 \quad n_3 \quad n_4 \quad n_\gamma/c \,]^T, \\
\mathbf{Q} &= \operatorname{diag}\{\, \sigma_{r_1}^2, \quad \sigma_{r_2}^2, \quad \sigma_{r_3}^2, \quad \sigma_{r_4}^2, \quad \sigma_{\gamma_e}^2/c^2 \,\}.
\end{aligned}
$$

A.3 Matrices for the 3D GALE Algorithm with Three TOA and One AOA Measurements

By incorporating the 3D AOA measurement (as defined in (3) and (4)) and the z-dimensional position estimate, matrices $\mathbf{H}$ and $\mathbf{J}$ in (10) can be augmented as

$$
\mathbf{H} = \begin{bmatrix} \mathbf{H}_{TOA}^{3\times 4} \\ \mathbf{H}_{AOA}^{2\times 4} \\ \mathbf{H}_{\gamma}^{1\times 4} \end{bmatrix} = \begin{bmatrix} -2x_1 & -2y_1 & -2z_1 & 1 \\ -2x_2 & -2y_2 & -2z_2 & 1 \\ -2x_3 & -2y_3 & -2z_3 & 1 \\ -\sin\theta & \cos\theta & 0 & 0 \\ 0 & 0 & \cos\phi & 0 \\ -2x_\gamma & -2y_\gamma & -2z_\gamma & 1 \end{bmatrix}, \tag{35}
$$

$$
\mathbf{J} = \begin{bmatrix} \mathbf{J}_{TOA}^{4\times 1} \\ \mathbf{H}_{AOA}^{2\times 1} \\ \mathbf{J}_{\gamma}^{1\times 1} \end{bmatrix} = \begin{bmatrix} r_1^2 - \kappa_1 \\ r_2^2 - \kappa_2 \\ -x_1\sin\theta + y_1\cos\theta \\ z_1 cos\phi + r_1\cos\phi\sin\phi \\ \gamma_e^2 - \kappa_\gamma \end{bmatrix}. \tag{36}
$$

Matrices $\mathbf{B}$, $\mathbf{n}$, and $\mathbf{Q}$ associated with the noise matrix ψ (as in (14)) can be obtained by

$$
\begin{aligned}
\mathbf{B} &= \operatorname{diag}\{\, \zeta_1, \quad \zeta_2, \quad \zeta_3, \quad \zeta_1\cos\phi, \quad \zeta_1, \quad \gamma \,\}, \\
\mathbf{n} &= [\, n_1 \quad n_2 \quad n_3 \quad n_\theta \quad n_\phi \quad n_\gamma/c \,]^T, \\
\mathbf{Q} &= \operatorname{diag}\{\, \sigma_{r_1}^2, \quad \sigma_{r_2}^2, \quad \sigma_{r_3}^2, \quad \sigma_\theta^2, \quad \sigma_\phi^2, \quad \sigma_{\gamma_e}^2/c^2 \,\}.
\end{aligned}
$$

ACKNOWLEDGMENTS

This work is supported in part by the MOE ATU Program 95W803C and the MediaTek Research Center at the National Chiao Tung University. The authors would like to thank the anonymous reviews for their constructive suggestions.

REFERENCES

[1] *Revision of the Commissions Rules to Insure Compatibility with Enhanced 911 Emergency Calling Systems,* Federal Communications Commission, 1996.

[2] S. Feng and C.L. Law, "Assisted GPS and Its Impact on Navigation in Intelligent Transportation Systems," *IEEE Intelligent Transportation Systems,* pp. 926-931, 2002.

[3] Y. Zhao, "Standardization of Mobile Phone Positioning for 3G Systems," *IEEE Comm. Magazine,* vol. 40, pp. 108-116, July 2002.

[4] H. Koshima and J. Hoshen, "Personal Locator Services Emerge," *IEEE Spectrum,* vol. 37, pp. 41-48, Feb. 2000.

[5] J.H. Reed, K.J. Krizman, B.D. Woerner, and T.S. Rappaport, "An Overview of the Challenges and Progress in Meeting the E-911 Requirement for Location Service," *IEEE Comm. Magazine,* vol. 36, pp. 30-37, Apr. 1998.

[6] X. Wang, Z. Wang, and B. O'Dea, "A TOA-Based Location Algorithm Reducing the Errors Due to Non-Line-of-Sight (NLOS) Propagation," *IEEE Trans. Vehicular Technology,* vol. 52, pp. 112-116, Jan. 2003.

[7] R.O. Schmidt, "Multiple Emitter Location and Signal Parameter Estimation," *IEEE Trans. Antennas and Propagation,* vol. 34, no. 3, pp. 276-280, Mar. 1986.

[8] E.G. Strom, S. Parkvall, S.L. Miller, and B.E. Ottersten, "Propagation Delay Estimation of DS-CDMA Signals in a Fading Environment," *Proc. IEEE Global Telecomm. Conf. (GLOBECOM '94),* pp. 85-89, Nov. 1994.

[9] P. Luukkanen and J. Joutsensalo, "Comparison of MUSIC and Matched Filter Delay Estimators in DS-CDMA," *Proc. Eighth IEEE Int'l Symp. Personal, Indoor, and Mobile Radio Comm. (PIMRC '97),* vol. 3, pp. 830-834, Sept. 1997.

[10] E.G. Strom, S. Parkvall, S.L. Miller, and B.E. Ottersten, "Propagation Delay Estimation in Asynchronous Direct-Sequence Code-Division Multiple Access Systems," *IEEE Trans. Comm.,* vol. 44, no. 1, pp. 84-93, Jan. 1996.

[11] S. Gazor, S. Affes, and Y. Grenier, "Robust Adaptive Beamforming via Target Tracking," *IEEE Trans. Signal Processing,* vol. 44, no. 6, pp. 1589-1593, June 1996.

[12] S. Affes, S. Gazor, and Y. Grenier, "An Algorithm for Multisource Beamforming and Multitarget Tracking," *IEEE Trans. Signal Processing,* vol. 44, no. 6, pp. 1512-1522, June 1996.

[13] K. Harmanci, J. Tabrikian, and J.L. Krolik, "Relationships between Adaptive Minimum Variance Beamforming and Optimal Source Localization," *IEEE Trans. Signal Processing,* vol. 48, no. 1, pp. 1-12, Jan. 2000.

[14] K. Kaemarungsi and P. Krishnamurthy, "Properties of Indoor Received Signal Strength for WLAN Location Fingerprinting," *IEEE Mobile and Ubiquitous Systems,* pp. 14-23, Aug. 2004.

[15] J. Kwon, B. Dundar, and P. Varaiya, "Hybrid Algorithm for Indoor Positioning Using Wireless LAN," *Proc. IEEE Vehicular Technology Conf. (VTC '04-Fall),* vol. 7, pp. 4625-4629, Sept. 2004.

[16] K. Kaemarungsi and P. Krishnamurthy, "Modeling of Indoor Positioning Systems Based on Location Fingerprinting," *Proc. IEEE INFOCOM,* vol. 2, pp. 1012-1022, Mar. 2004.

[17] A.J. Weiss, "On the Accuracy of a Cellular Location System Based on RSS Measurements," *IEEE Trans. Vehicular Technology,* vol. 52, no. 6, pp. 1508-1518, Nov. 2003.

[18] J. Zhu and G.D. Durgin, "Indoor/Outdoor Location of Cellular Handsets Based on Received Signal Strength," *IEEE Electronics Letters,* vol. 41, no. 1, pp. 24-26, Jan. 2005.

[19] T. Imai and T. Fujii, "Indoor Micro Cell Area Prediction System Using Ray-Tracing for Mobile Communication Systems," *Proc. Seventh IEEE Int'l Symp. Personal, Indoor, and Mobile Radio Comm. (PIMRC '97),* vol. 1, pp. 24-28, Oct. 1996.

[20] K.R. Chang and H.T. Kim, "Improvement of the Computation Efficiency for a Ray-Launching Model," *IEEE Antennas and Propagation,* vol. 145, no. 4, pp. 303-308, Aug. 1998.

[21] S.T. Tan and H.S. Tan, "Improved Three-Dimensional Ray Tracing Technique for Microcellular Propagation Models," *IEEE Electronics Letters,* vol. 31, no. 17, pp. 1503-1505, Aug. 1995.

[22] Z. Sandor, L. Nagy, Z. Szabo, and T. Csaba, "3D Ray Launch and Moment Method for Indoor Radio Propagation Purposes," *Proc. Seventh IEEE Int'l Symp. Personal, Indoor, and Mobile Radio Comm. (PIMRC '97),* vol. 1, pp. 130-134, Sept. 1997.

[23] M. Hata, "Empirical Formula for Propagation Loss in Land Mobile Radio Services," *IEEE Trans. Vehicular Technology,* vol. 29, no. 3, pp. 317-325, Aug. 1980.

[24] S.Y. Seidal and T.S. Rappaport, "Site Specific Propagation Prediction for Wireless In-Building Personal Communication System Design," *IEEE Trans. Vehicular Technology,* vol. 43, no. 4, pp. 879-891, Nov. 1994.

[25] W.H. Foy, "Position-Location Solutions by Taylor-Series Estimation," *IEEE Trans. Aerospace and Electronic Systems,* vol. 12, pp. 187-194, Mar. 1976.
[26] W. Wang, J.Y. Xiong, and Z.L. Zhu, "A New NLOS Error Mitigation Algorithm in Location Estimation," *IEEE Trans. Vehicular Technology,* vol. 54, pp. 2048-2053, Nov. 2005.
[27] Y.T. Chan and K.C. Ho, "A Simple and Efficient Estimator for Hyperbolic Location," *IEEE Trans. Signal Processing,* vol. 42, pp. 1905-1915, 1994.
[28] L. Cong and W. Zhuang, "Hybrid TDOA/AOA Mobile User Location for Wideband CDMA Cellular Systems," *IEEE Trans. Wireless Comm.,* vol. 1, pp. 439-447, July 2002.
[29] J. Caffery Jr., "A New Approach to the Geometry of TOA Location," *Proc. IEEE Vehicular Technology Conf. (VTC '00-Fall),* vol. 4, pp. 1943-1949, Sept. 2000.
[30] S. Venkatraman and J. Caffery Jr., "Hybrid TOA/AOA Techniques for Mobile Location in Non-Line-of-Sight Environments," *Proc. IEEE Wireless Comm. and Networking Conf. (WCNC '04),* vol. 1, no. 6, pp. 274-278, Mar. 2004.
[31] J.F. Liao and B.S. Chen, "Robust Mobile Location Estimator with NLOS Mitigation Using Interacting Multiple Model Algorithm," *IEEE Trans. Wireless Comm.,* vol. 5, no. 11, pp. 3002-3006, Nov. 2006.
[32] S. Venkatraman, J. Caffery Jr., and H.R. You, "A Novel ToA Location Algorithm Using LoS Range Estimation for NLoS Environments," *IEEE Trans. Vehicular Technology,* vol. 53, no. 5, pp. 1515-1524, Sept. 2004.
[33] T. Rantalainen, "Mobile Station Emergency Location in GSM," *Proc. IEEE Int'l Conf. Personal Wireless Comm. (PWC '96),* pp. 232-238, Feb. 1996.
[34] M.P. Wylie and J. Holtzman, "The Non-Line of Sight Problem in Mobile Location Estimation," *Proc. Fifth IEEE Int'l Conf. Universal Personal Comm. (IUPC '96),* vol. 2, pp. 827-831, 1996.
[35] The CDMA ITU-R RTT Candidate Submission (0.18), June 1998.
[36] Japans Proposal for Candidate Radio Transmission Technology on IMT-2000: W-CDMA, June 1998.
[37] L.J. Greenstein, V. Erceg, Y.S. Yeh, and M.V. Clark, "A New Path-Gain/Delay-Spread Propagation Model for Digital Cellular Channels," *IEEE Trans. Vehicular Technology,* vol. 46, pp. 477-485, May 1997.
[38] C.Y. Lee, *Mobile Communications Engineering.* McGraw-Hall, 1993.
[39] R.E. Blahut, *Principles and Practice of Information Theory,* chapter 8. Addison-Wesley, 1987.
[40] K.W. Cheung, H.C. So, W.K. Ma, and B.D. Woemer, "Received Signal Strength Based Mobile Positioning via Constrained Weighted Least Squares," *Proc. IEEE Int'l Conf. Acoustics, Speech, and Signal Processing (ICASSP '03),* vol. 5, pp. 137-140, 2003.
[41] N. Levanon, "Lowest GDOP in 2-D Scenarios," *IEE Proc.—Radar, Sonar and Navigation,* vol. 147, pp. 149-155, June 2002.

Kai-Ten Feng received the BS degree from the National Taiwan University, Taipei, in 1992, the MS degree from the University of Michigan, Ann Arbor, in 1996, and the PhD degree from the University of California, Berkeley, in 2000. Since February 2003, he has been with the Department of Communication Engineering, National Chiao Tung University, Hsinchu, Taiwan, as an assistant professor. He was with OnStar Corporation USA, a subsidiary of General Motors Corporation, as an in-vehicle development manager/senior technologist from 2000 to 2003. His major responsibilities with OnStar included the design of future telematics platforms and the in-vehicle networks. His current research interests include mobile ad hoc networks, wireless location technologies, wireless sensor networks, embedded system design, and Intelligent Transportation Systems (ITSs). He received the Best Paper Award from the IEEE Vehicular Technology Conference Spring 2006, which was ranked as the first among the 615 accepted papers. He has served on the technical program committees in the IEEE Vehicular Technology Conference (VTC), IEEE VTS Asia Pacific Wireless Communications Symposium (APWCS), and International Conference on Communications, Circuits and Systems (ICCCAS). He is a member of the IEEE.

Chao-Lin Chen received the BS and MS degrees in communication engineering from the National Chiao Tung University, Hsinchu, Taiwan, in 2003 and 2006. He is currently with the Department of Electronics Engineering, National Chiao Tung University, Hsinchu, Taiwan, as a teaching assistant. His current research interests include wireless location technologies and wireless sensor networks.

Chien-Hua Chen received the BS degree in electrical engineering from the National Cheng Kung University, Tainan, Taiwan, in 2002 and the MS degree in communication engineering from the National Chiao Tung University, Hsinchu, Taiwan, in 2006. Since 2006, he has been working toward the PhD degree in the Department of Communication Engineering, National Chiao Tung University, Hsinchu, Taiwan. His current research interests include wireless location technologies and message access control (MAC) layer issues for Wi-Fi systems. He is a student member of the IEEE.